Nanoscale Res Lett (2009) 4:78–83
DOI 10.1007/s11671-008-9205-6

NANO EXPRESS

Synthesis and Luminescence Properties of Core/Shell ZnS:Mn/ZnO Nanoparticles

Daixun Jiang · Lixin Cao · Wei Liu · Ge Su · Hua Qu · Yuanguang Sun · Bohua Dong

Received: 18 September 2008 / Accepted: 30 October 2008 / Published online: 26 November 2008

Abstract In this paper the influence of ZnO shell thickness on the luminescence properties of Mn-doped ZnS nanoparticles is studied. Transmission electron microscopy (TEM) images showed that the average diameter of ZnS:Mn nanoparticles is around 14 nm. The formation of ZnO shells on the surface of ZnS:Mn nanoparticles was confirmed by X-ray diffraction (XRD) patterns, high-resolution TEM (HRTEM) images, and X-ray photoelectron spectroscopy (XPS) measurements. A strong increase followed by a gradual decline was observed in the room temperature photoluminescence (PL) spectra with the thickening of the ZnO shell. The photoluminescence excitation (PLE) spectra exhibited a blue shift in ZnO-coated ZnS:Mn nanoparticles compared with the uncoated ones. It is shown that the PL enhancement and the blue shift of optimum excitation wavelength are led by the ZnO-induced surface passivation and compressive stress on the ZnS:Mn cores.

Keywords ZnS:Mn/ZnO · Nanoparticles · Core/shell structure · Luminescence · II-VI Semiconductor

Introduction

In recent years, a great deal of attention has been devoted to doped semiconductor nanomaterials mainly due to their unique luminescence properties arising from quantum confinement effects. The doping ions act as recombination centers for the excited electron–hole pairs and play an influential role in determining optical properties, resulting in strong luminescence. Among the semiconductor nanomaterials, zinc sulfide is particularly suitable for use as luminescent host materials for a variety of dopants because of its wide band gap energy at room temperature. There have been numerous reports about the structural and luminescence properties of doped ZnS nanocrystals, such as ZnS nanocrystals doped with manganese [1–4], copper [5–7], silver [8], samarium [9], europium [10, 11], and terbium [12]. It has been extensively studied for a variety of commercial devices, such as electro-optic modulators, photoconductors, optical coatings, field effect transistors, infrared windows, electroluminescent display [13–17]. Unfortunately, serious drawbacks exist in these nanomaterials, such as their instability under high temperature treatment [18], degradation during the operation and dispersal into vacuum, which will contaminate the field emitter and thus hinder the electron emission [19], and high surface-to-volume ratio because of small particle size, which will result in low luminescence efficiency. In order to conquer such serious shortcomings, accordingly, core/shell structural nanomaterials have been developed and have shown dramatically enhanced properties. Enhanced luminescence and/or stability has been observed in ZnS:Mn/SiO_2 nanoparticles [20], ZnS:Mn/ZnS nanocrystals [21], ZnS:Mn/$Zn(OH)_2$ nanoparticles [22], ZnS:Mn/ZnO nanocrystals [23], and CdSe/ZnO nanoparticles [24]. In addition, the ZnO particles on the ZnS:Ag particulates have demonstrated a high effectiveness to prevent the degradation of ZnS:Ag particulates from electron bombardment [25]. Compared with the uncoated nanocrystals, the photoluminescence of the nanocrystals with a core/shell structure is enhanced. This is usually interpreted as being due to the surface passivation that inhibits the nonradiative

D. Jiang · L. Cao (✉) · W. Liu · G. Su · H. Qu · Y. Sun · B. Dong
Institute of Materials Science and Engineering, Ocean University of China, Qingdao 266100, People's Republic of China
e-mail: caolixin@mail.ouc.edu.cn

recombination, thus improving the photoluminescence properties. At the same time, a higher stability will be obtained, coming from the protection effect of the surrounding matrix [26].

ZnO-coated ZnS:Mn nanoparticles have been prepared by different groups [23, 27]; however, the ZnO shells reported in these literatures are of rather poor crystallinity, which is indicated by their X-ray diffraction (XRD) results. Usually, the ZnO shell with higher crystallinity will produce stress on the ZnS:Mn because of the lattice mismatch, and bring efficient luminescent transitions inducing enhanced luminescence [28]. In this paper, a convenient route to prepare higher crystallinity core/shell structural ZnS:Mn/ZnO nanoparticles is reported, with the emphasis on the improved luminescence properties brought by the ZnO capping on the ZnS:Mn nanoparticles. The shell material, ZnO, is a wide band gap semiconductor with excellent chemical and thermal stability. Therefore, surface modification of ZnS:Mn nanoparticles by ZnO shell is expected to have a passivating effect on the surface states of ZnS:Mn, which would result in enhanced luminescence.

Experimental Details

All the reactants and solvents used in this work were of analytical grade and used without any further purification.

Synthesis of ZnS:Mn Cores

Typically, 0.01 mol zinc acetate [$Zn(CH_3COO)_2 \cdot 2H_2O$], 0.005 mol thioacetamide [CH_3CSNH_2], and 5×10^{-5} mol manganese acetate [$Mn(CH_3COO)_2 \cdot 4H_2O$] were put into a Teflon-lined stainless steel autoclave of 72 mL capacity, and then the autoclave was filled with a mixture solvent of ethylenediamine and deionized water (in 1:1 volume ratio) to 80% of its total volume. Then the reactants and solvents were stirred for 20 min. After being sealed, the autoclave was maintained at 200 °C for 6 h and then cooled down to room temperature naturally. The final precipitates were separated by centrifugation at 5000 rpm and washed with deionized water and absolute ethanol three times to remove excessive ethylenediamine and by-products. The samples were then dried in vacuum at 50 °C for 5 h and collected for further characterization and treatment.

Surface Synthesis of ZnO Shells on ZnS:Mn Cores

In order to make ZnO shells coating on ZnS:Mn nanocrystals, the reaction between $Zn(NO_3)_2$ and NaOH was employed. In a typical process, 0.2 g bare ZnS:Mn nanocrystals powder was put into 200 mL deionized water and ultrasonically dispersed for 1 h, followed by slow dropping of appropriate amount of 0.05 M $Zn(NO_3)_2$ aqueous solution into the ZnS:Mn suspension under vigorous stirring. Drops of 0.1 M NaOH aqueous solution were then slowly added until the pH value arrived at $\sim$10 [29], at which point ZnO precipitated at the surface of the ZnS:Mn nanocrystals. The nucleation and growth of a separate ZnO particle were suppressed by the very low concentration of NaOH in the ZnS:Mn suspension in the dropping process. The resulting precipitates were dealt with in the same procedure as that for ZnS:Mn nanocrystals. The thickness of ZnO shell was controlled by varying the dosage of $Zn(NO3)_2$, as indicated in Table 1.

Table 1 Dosage of $Zn(NO_3)_2$ aqueous solution (0.05 M) used in forming ZnO shells. (In the parentheses, 0, 0.1, 0.2, 0.3, 0.4, 0.5 and 1 are set to be the mole ratios of Zn^{2+} ions in shells and cores)

Samples	Volume of $Zn(NO_3)_2$ aqueous solution (mL)
ZnS:Mn/ZnO(0)	0
ZnS:Mn/ZnO(0.1)	10
ZnS:Mn/ZnO(0.2)	20
ZnS:Mn/ZnO(0.3)	30
ZnS:Mn/ZnO(0.4)	40
ZnS:Mn/ZnO(0.5)	50
ZnS:Mn/ZnO(1)	100

Characterization

The X-ray diffraction patterns of as-synthesized ZnS:Mn/ZnO nanoparticles were collected on a D8 ADVANVCE X-Ray diffractometer. A JEM-2100 transmission electron microscope (TEM) was used to study the morphologies of the samples. The room temperature photoluminescence (PL) spectra were achieved by a Flurolog-3p fluorescence spectrophotometer. The X-ray photoelectron spectroscopy (XPS) measurements made on the samples with and without sputtering were performed on ESCA MK II.

Results and Discussion

Structural Characterization

The X-ray diffraction results are plotted in Fig. 1. Figure 1a shows the XRD patterns of the uncoated ZnS:Mn nanocrystals. The four diffraction peaks can be indexed as (111), (200), (220), and (311) planes of cubic zinc blende structure, which match well with the standard card (JCPDS NO. 05-0566). The XRD patterns of some representative core/shell structural ZnS:Mn/ZnO nanoparticles are presented in Fig. 1b–e. From Fig. 1b, it can be found that there are almost no XRD peaks from crystalline ZnO,

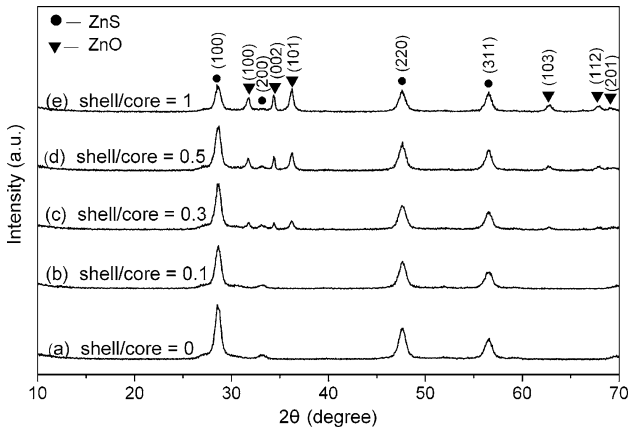

Fig. 1 XRD patterns of ZnS:Mn nanoparticles **a** without and **b–e** with ZnO shells of different thicknesses

indicating that the amount of ZnO is very low in this sample. Compared with the bare ZnS:Mn core, some new diffraction peaks appear in Fig. 1c–e, which centered at about 31.7°, 34.4°, 36.2°, 62.8°, 67.9°, and 69.0°. These peaks correspond to (100), (002), (101), (103), (112) and (201) diffraction peaks from the standard card (JCPDS NO. 80-0074), respectively, indicating that the ZnO shells possess a wurtzite structure. From the XRD results, it can be clearly observed that the intensity of the diffraction peaks from ZnO becomes stronger progressively, providing evidence for the gradual increase in the amount of ZnO shell as planed.

Figure 2a, b shows two typical TEM images of ZnS:Mn nanoparticles without and with ZnO shell. From Fig. 2a, we can see that the as-synthesized ZnS:Mn nanoparticles are spherical, with an average diameter of about 14 nm. In comparison with Fig. 2a, it can be seen in Fig. 2b that the ZnS:Mn nanoparticles coated with a ZnO shell (shell/core = 1) are almost kept unchanged in average diameter. This is possibly because the thickness of ZnO shell is too thin to induce an obvious change in particle size. Figure 2c shows the high-resolution TEM (HRTEM) image of a single ZnS:Mn nanoparticle. From the figure, the lattice spacing was calculated to be around 0.32 nm, which corresponds to the (111) lattice plane spacing of ZnS in cubic phase. HRTEM investigations of core/shell ZnS:Mn/ZnO(1) (Fig. 2d) show the interface between ZnO shell and ZnS:Mn core. The two measured distances between adjacent lattice fringes are 0.26 and 0.32 nm, which correspond to the (002) lattice plane of a hexagonal ZnO crystal and the (111) lattice plane of a cubic ZnS crystal, respectively.

The surface sensitivity of XPS can be used to indicate whether or not the ZnO covers the outer surface of ZnS:Mn nanocrystal [30]. XPS survey spectrum of sample ZnS:Mn/ZnO(0.5) is plotted in Fig. 3a. The peaks located at 1,021.6, 532.1, and 162.2 eV correspond to $Zn2p_{3/2}$, O1s, and S2p, respectively. Displayed in Fig. 3b, c and d are the finely scanned $Zn2p_{3/2}$, O1s, and S2p peaks of ZnS:Mn/ZnO(0.5), respectively.

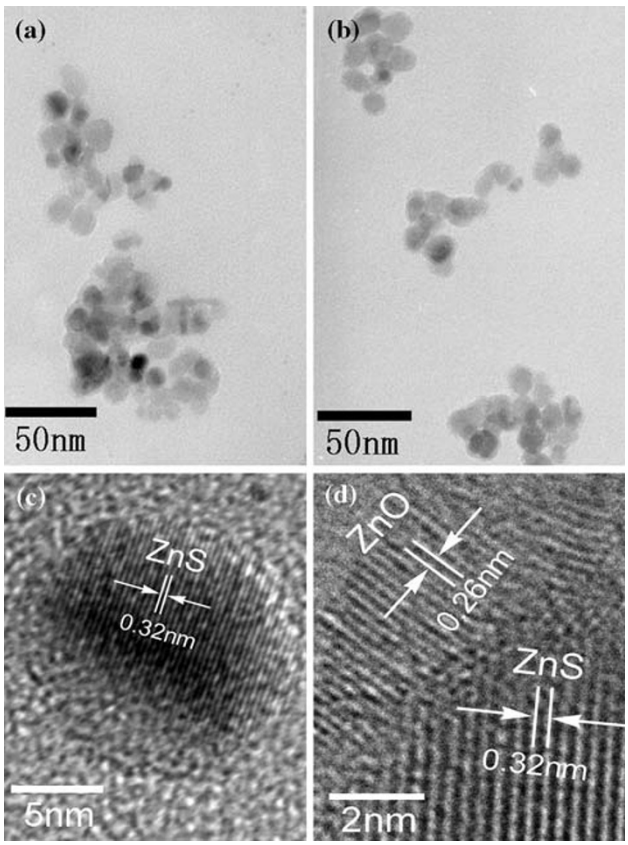

Fig. 2 TEM images of ZnS:Mn and ZnS:Mn/ZnO nanoparticles. **a** ZnS:Mn. **b** ZnS:Mn/ZnO(1). **c** HRTEM iamge of a single ZnS:Mn nanoparticle. **d** HRTEM image of ZnS:Mn/ZnO(1) nanoparticle showing the interface between shell and core

In order to show further evidence that ZnO covers on the outer surface, XPS measurements were carried out on ZnS:Mn/ZnO(0.5) with and without sputtering (Fig. 4). The atomic ratio of oxygen to sulfur can be calculated by dividing the area of the XPS peaks by their respective sensitivity factors (2.93 for O and 1.68 for S) [31]. As shown in Fig. 4, the oxygen to sulfur atomic ratio first decreases gradually and remains almost invariant thereafter with increasing sputtering time, which confirms the presence of ZnO shell on the outer surface of ZnS:Mn cores [23].

Photoluminescence Properties

The room temperature photoluminescence emission (PL) and excitation (PLE) spectra of all samples are plotted in Fig. 5 and Fig. 6. In Fig. 5, the PL spectra of all samples present two emission bands. The orange emission, with a peak wavelength of ~580 nm, is attributed to the

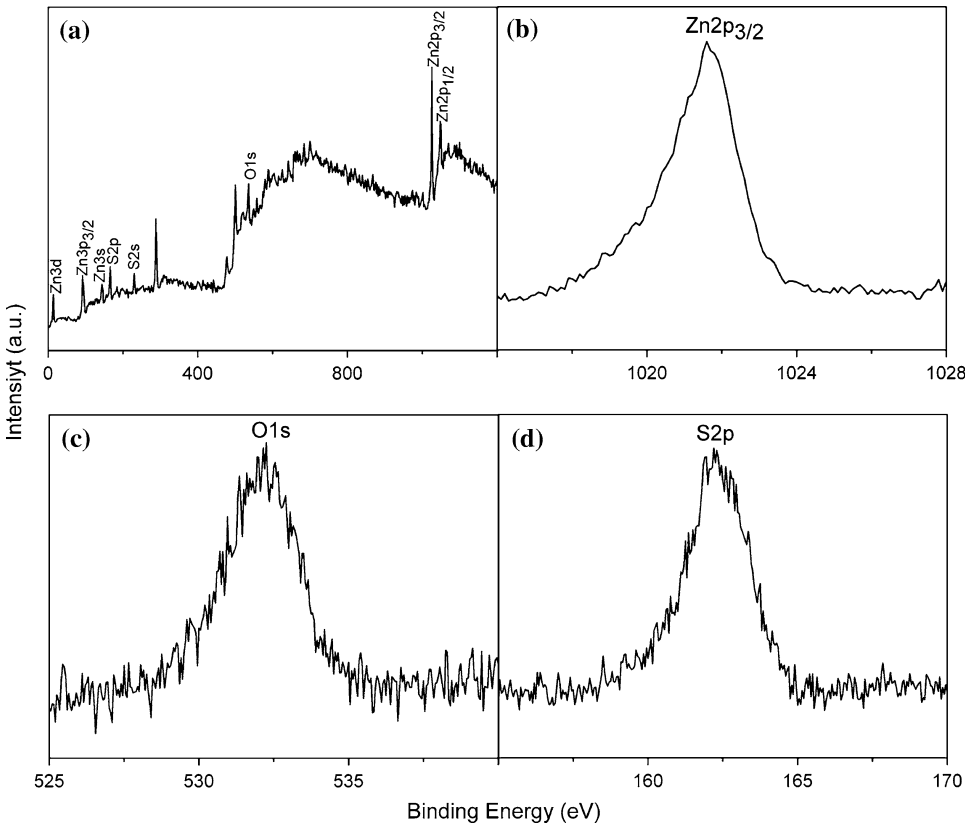

Fig. 3 XPS spectra of sample ZnS:Mn/ZnO(0.5). **a** Survey spectrum. **b** Zn 2p3/2 spectrum; **c** O1s spectrum. **d** S2p spectrum

transition from $^4T_1$ (excited) to $^6A_1$ (ground) of Mn^{2+} ions [2], indicating that the Mn^{2+} ions have been successfully incorporated into the ZnS host lattice [32]. The green emission with its maximum at ~500 nm is due to self-activated defect centers formed by the zinc vacancy inside the lattice [33, 34]. The emission at ~500 nm is rather weak in contrast to that at ~580 nm, demonstrating the highly crystalline quality of ZnS:Mn nanocrystals [35], which agrees well with the XRD results. The orange emission intensity of ZnS:Mn/ZnO nanocrystals first increases and then decreases with the thickening of the ZnO shells, and the green emission is also enhanced after coating the ZnS:Mn cores with ZnO shells. A small blue shift can be observed in the ZnS:Mn/ZnO composites when compared with the uncoated ZnS:Mn nanocrystals. These show that ZnO shells have great effect on the photoluminescence properties of ZnS:Mn nanocrystals. Generally, for the uncoated ZnS:Mn nanoparticles, some Mn^{2+} ions

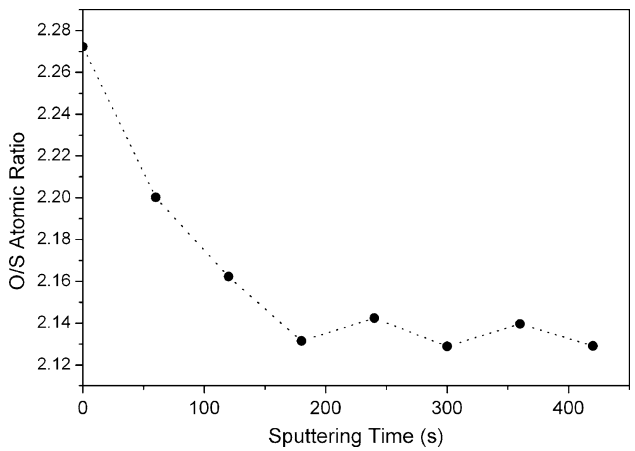

Fig. 4 Representative XPS spectrum of sample ZnS:Mn/ZnO(0.5) showing relative change in O/S atomic ratio with sputtering time

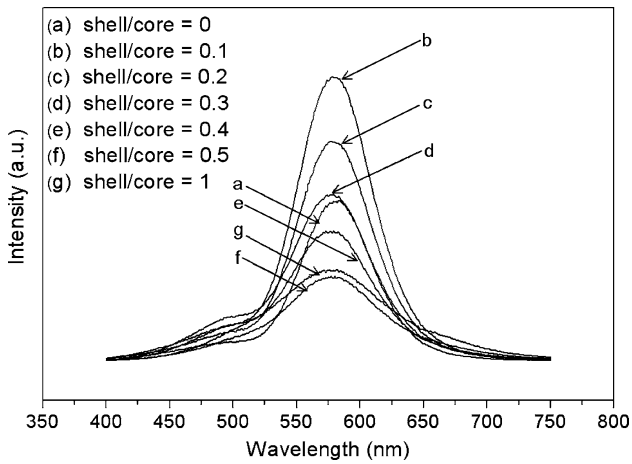

Fig. 5 PL spectra excited at 350 nm of ZnS:Mn nanoparticles **a** without and **b–g** with ZnO shells of different thickness

distribute on the surface and form some nonradiative recombination routes from surface Mn^{2+} ions to surface quenching centers, which will bring reduction in the PL intensity. Therefore, the luminescence is weak. When ZnO shells form on the surface of ZnS:Mn nanocrystals, the distance from Mn^{2+} ions to the surface of nanocrystal will increase, which can weaken the energy transferred to the surface quenching centers. Hence, the PL intensity of Mn^{2+} ions transition was enhanced through the increase of radiative transition of Mn^{2+} ions. In addition, the compressive stress due to the lattice mismatch between ZnS core and ZnO shell will shift luminescent energy levels of ZnS to higher energy regions producing more efficient luminescent transitions, which was a possible reason for the luminescence enhancement [28]. On the other hand, the concentration of luminescent center (Mn^{2+} ions) was gradually reduced with increasing thickness of the ZnO shell, and this would therefore decrease the intensity of Mn emission. It is, accordingly, understandable that the PL intensity of Mn emission first increases and then decreases with the thickening of the ZnO shells due to the opposite effects of ZnO shells on ZnS:Mn nanoparticles. According to literatures, the enhancement of green emission at ~500 nm is caused by the removal of electron capture centers on the surface of ZnS:Mn nanocrystals or the removal of nonradiative decay channels due to the ZnO shells [19]. Moreover, it is also a possible reason for the potential increasing of the Zn vacancy as a result of the dropping process of NaOH aqueous solution [34]. The photoluminescence quantum yield (PLQY) was measured against rhodamine as standard, and the values for bare ZnS:Mn, ZnS:Mn/ZnO(0.1), and ZnS:Mn/ZnO(1) are 0.042, 0.19, and 0.034%, respectively.

In Fig. 6, the excitation spectra monitoring the characteristic emission of Mn^{2+} ions show a broad band with a peak at ~350 nm, which is the characteristic peak of ZnS absorption. It demonstrates that the emission of transition from $^4T_1$ to $^6A_1$ of Mn^{2+} ions takes place via the energy transfer from the excited ZnS host lattice to Mn^{2+} ions. Compared with the uncoated ZnS:Mn nanoparticles, a blue shift shown in the PLE spectra of ZnS:Mn/ZnO(0.1) and ZnS:Mn/ZnO(0.2) is slight (Fig. 5b, c), which is dramatic for ZnS:Mn/ZnO(0.3), ZnS:Mn/ZnO(0.4), ZnS:Mn/ZnO(0.5), and ZnS:Mn/ZnO(1) (Fig. 5d, e, f, and g). Such a blue shift has also been observed in the ZnS:Mn nanocrystals after surface passivation by silica [20]. In addition, it has been reported that the strain between core and shell in such core/shell semiconductor nanocomposites will broaden the band gap of the core, resulting in a blue shift of the emitted energy [36, 37]. Hence, a possible mechanism that can explain the observed blue shift in this excitation spectra is as follows: The stress caused by the lattice mismatch between ZnO and ZnS can alter the ZnS lattice parameters slightly [28], and further influence the energy level structure of ZnS host, resulting in the shift of excitation spectra to shorter wavelength. This differs from the previous report where ZnS:Mn nanocrystals coated by ZnO shell showed a red shift in comparison with the uncoated ones in PLE spectra [27]. The distinction is presumably due to the higher crystallinity of the ZnO shells reported here, which will result in lattice mismatch with ZnS cores producing compressive stress as discussed above, and the stress should be responsible for the blue shift in the PLE spectra. However, details of this phenomenon are not very clear at this stage.

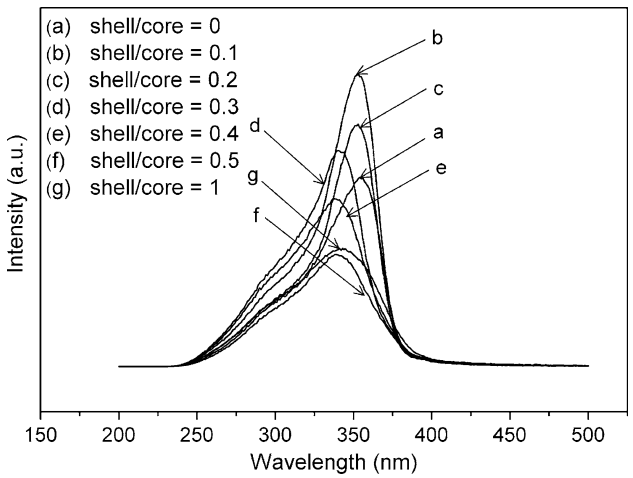

Fig. 6 PLE spectra monitored at 580 nm of ZnS:Mn nanoparticles **a** without and **b–g** with ZnO shells of different thicknesses

Conclusion

Core/shell ZnS:Mn/ZnO nanoparticles were successfully synthesized, and their structural and luminescence properties were investigated. XRD, HRTEM, and XPS results reinforced the claim that ZnO shells were coated on the surface of ZnS:Mn cores. Compared with the uncoated ZnS:Mn nanoparticles, the Mn emission intensity of ZnO-coated ZnS:Mn showed a strong increase followed by a gradual decline, which was led by the opposite effects of ZnO shells, i.e., surface passivation inducing luminescence enhancement and decrease of the luminescent centers (Mn^{2+} ions) inducing luminescence weakening. The obvious blue shift observed in the PLE spectra was caused by the ZnO-induced compressive stress on the ZnS:Mn cores.

Acknowledgments The authors thank the National Science Foundation of China (NSFC 50672089) and the Encouraging Foundation for the Scientific Research of the Excellent Young and Middle-aged Scientists in Shandong Province (2006BS04034) for financial support.

References

1. J.F. Suyver, S.F. Wuister, J.J. Kelly, A. Meijerink, Nano. Lett. **1**, 429 (2001). doi:10.1021/nl015551h
2. B. Xia, I.W. Lenggoro, K. Okuyama, Chem. Mater. **14**, 4969 (2002). doi:10.1021/cm020409i
3. S. Sapra, A. Prakash, A. Ghangrekar, N. Periasamy, D.D. Sarma, J. Phys. Chem. B **109**, 1663 (2005). doi:10.1021/jp049976e
4. R. Tu, B. Liu, Z. Wang, D. Gao, F. Wang, Q. Fang, Z. Zhang, Anal. Chem. **80**, 3458 (2008). doi:10.1021/ac800060f
5. O. Ehlert, A. Osvet, M. Batentschuk, A. Winnacker, T. Nann, J. Phys. Chem. B **110**, 23175 (2006). doi:10.1021/jp064570i
6. D. Kima, K.D. Min, J. Lee, J.H. Park, J.H. Chun, Mater. Sci. Eng. B **131**, 13 (2006). doi:10.1016/j.mseb.2005.11.005
7. N. Karar, Solid State Commun. **142**, 261 (2007). doi:10.1016/j.ssc.2007.02.023
8. W. Jian, J. Zhuang, D. Zhang, J. Dai, W. Yang, Y. Bai, Mater. Chem. Phys. **99**, 494 (2006). doi:10.1016/j.matchemphys.2005.11.030
9. T. Kushida, A. Kurita, M. Watanabe, Y. Kanematsu, K. Hirata, N. Okubo, Y. Kanemitsu, J. Lumin. **87–89**, 466 (2000). doi:10.1016/S0022-2313(99)00493-7
10. W. Chen, J.O. Malm, V. Zwiller, Y. Huang, S. Liu, R. Wallenberg, J.O. Bovin, L. Samuelson, Phys. Rev. B **61**, 11021 (2000). doi:10.1103/PhysRevB.61.11021
11. S.C. Qu, W.H. Zhou, F.Q. Liu, N.F. Chen, Z.G. Wang, H.Y. Pan, D.P. Yu, Appl. Phys. Lett. **80**, 3605 (2002). doi:10.1063/1.1478152
12. C. Tiseanu, R.K. Mehra, R. Kho, M. Kumke, J. Phys. Chem. B **107**, 12153 (2003). doi:10.1021/jp035322e
13. W. Tang, D.C. Cameron, Thin Solid Films **280**, 221 (1996). doi:10.1016/0040-6090(95)08198-4
14. M. Bredol, J. Merikhi, J. Mater. Sci. **33**, 471 (1998). doi:10.1023/A:1004396519134
15. N. Karar, F. Singh, B.R. Mehta, J. Appl. Phys. **95**, 656 (2004). doi:10.1063/1.1633347
16. Y. Ding, X.D. Wang, Z.L. Wang, Chem. Phys. Lett. **398**, 32 (2004). doi:10.1016/j.cplett.2004.09.031
17. A.B. Cruz, Q. Shen, T. Toyoda, Mater. Sci. Eng. C **25**, 761 (2005). doi:10.1016/j.msec.2005.06.022
18. J. Mu, D.Y. Gu, Z.Z. Xu, Mater. Res. Bull. **40**, 2198 (2005). doi:10.1016/j.materresbull.2005.06.014
19. Y. Zhang, Y.D. Li, J. Phys. Chem. B **108**, 17805 (2004). doi:10.1021/jp047446c
20. Y. Hattori, T. Isobe, H. Takahashi, S. Itoh, J. Lumin. **113**, 69 (2005). doi:10.1016/j.jlumin.2004.08.054
21. L.X. Cao, J.H. Zhang, S.L. Ren, S.H. Huang, Appl. Phys. Lett. **80**, 4300 (2002). doi:10.1063/1.1483113
22. D.X. Jiang, L.X. Cao, G. Su, H. Qu, D.K. Sun, Appl. Surf. Sci. **253**, 9330 (2007). doi:10.1016/j.apsusc.2007.05.067
23. N. Karar, H. Chander, S.M. Shivaprasad, Appl. Phys. Lett. **85**, 5058 (2004). doi:10.1063/1.1815059
24. G.Y. Shan, X.G. Kong, X. Wang, Y.C. Liu, Surf. Sci. **582**, 61 (2005). doi:10.1016/j.susc.2005.02.055
25. H.H. Choi, M. Ollinger, R.K. Singh, Appl. Phys. Lett. **82**, 2494 (2003). doi:10.1063/1.1567040
26. M.A. Hines, P.G. Sionnest, J. Phys. Chem. **100**, 468 (1996). doi:10.1021/jp9530562
27. A.D. Dinsmore, D.S. Hsu, S.B. Qadri, J.O. Cross, T.A. Kennedy, H.F. Gray, B.R. Ratna, J. Appl. Phys. **88**, 4985 (2000). doi:10.1063/1.1314326
28. D. Haranath, H. Chander, N. Bhalla, P. Sharma, K.N. Sood, Appl. Phys. Lett. **86**, 201904 (2005). doi:10.1063/1.1929076
29. S. Amabi, H. Imai, J. Mater. Chem. **12**, 3773 (2002). doi:10.1039/b205384e
30. H. Yang, P.H. Holloway, J. Chem. Phys. **121**, 7421 (2004). doi:10.1063/1.1797071
31. B.O. Dabbousi, J.R. Viejo, F.V. Mikulec, J.R. Heine, H. Mattoussi, R. Ober, K.F. Jensen, M.G. Bawendi, J. Phys. Chem. B **101**, 9463 (1997). doi:10.1021/jp971091y
32. H. Hu, W.H. Zhang, Opt. Mater. **28**, 536 (2006). doi:10.1016/j.optmat.2005.03.015
33. S. Biswas, S. Kar, S. Chaudhuri, J. Phys. Chem. B **109**, 17526 (2005). doi:10.1021/jp053138i
34. N. Murase, R. Jagannathan, Y. Kanematsu, M. Watanabe, A. Kurita, K. Hirata, T. Yazawa, T. Kushida, J. Phys. Chem. B **103**, 754 (1999). doi:10.1021/jp9828179
35. Y.Q. Li, J.A. Zapien, Y.Y. Shan, Y.K. Liu, S.T. Lee, Appl. Phys. Lett. **88**, 013115 (2006). doi:10.1063/1.2161073
36. Z. Zanolli, L.E. Fröberg, M.T. Björk, M.E. Pistol, L. Samuelson, Thin Solid Films **515**, 793 (2006). doi:10.1016/j.tsf.2005.12.199
37. H.M. Lin, Y.L. Chen, J. Yang, Y.C. Liu, K.M. Yin, J.J. Kai, F.R. Chen, L.C. Chen, Y.F. Chen, C.C. Chen, Nano. Lett. **3**, 537 (2003). doi:10.1021/nl0340125